Journal of Medicinal Chemistry

ARTICLE

pubs.acs.org/jmc

Peptide-Based Imaging Agents Targeting Phosphatidylserine for the Detection of Apoptosis

Chiyi Xiong, Kari Brewer, Shaoli Song, Rui Zhang, Wei Lu, Xiaoxia Wen, and Chun Li*

Department of Experimental Diagnostic Imaging, The University of Texas M. D. Anderson Cancer Center, 1515 Holcombe Boulevard, Houston, Texas 77030, United States

ABSTRACT:

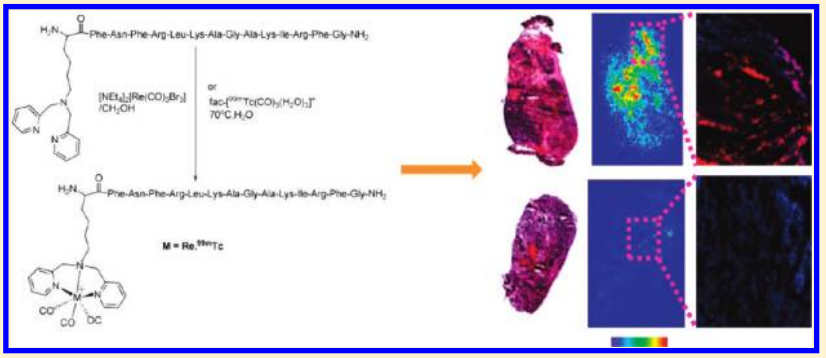

A 14-residue phosphatidylserine (PS)-binding peptide FNFRLKAGQKIRFG (PSBP-0) was scanned with Ala. In addition, a radiometal chelator (SAAC) was introduced at selected sites of the lead peptides. Substitution of the Gln[6] residue in PSBP-0 with Ala resulted in a significant increase in binding affinity to PS as determined by surface plasmon resonance sensorgrams. The binding affinity of the resulting peptide FNFRLKAGAKIRFG (PSBP-6, molecular mass = 1623 Da) to PS ($K_d \sim 100$ nM) increased 10-fold as compared to PSBP-0 ($K_d \sim 1.38$ μM). Introduction of SAAC-Re to the N terminus of PSBP-6 further increased the binding affinity of the resulting peptide SAAC(Re)-PSBP-6 ($K_d \sim 26$ nM). SAAC(Re)-PSBP-6 shows specific binding to apoptotic cells in cell-based assays. Biodistribution studies showed significantly higher uptake of SAAC($^{99\ m}$Tc)-PSBP-6 in B16/F10 melanoma treated with poly(L-glutamic acid)-paclitaxel than untreated tumors (4.06 $\pm$ 0.55% ID/g vs 1.61 $\pm$ 0.33% ID/g, $P = 0.00011$). SAAC($^{99\ m}$Tc)-PSBP-6 is a promising probe for noninvasive imaging of apoptotic cells.

INTRODUCTION

Apoptosis, or programmed cell death, is a specialized form of cell death involved in a wide variety of physiological and pathological processes.[1,2] In cancer, the balance between cell proliferation and apoptosis shifts toward cell proliferation; thus, most anticancer therapeutic regimens induce apoptosis. New anticancer therapies are being developed to induce apoptosis and to inhibit tumor growth.[3,4] Accurate assessment and monitoring of response to proapoptotic interventions is critical for the optimal care of cancer patients. The ability to monitor apoptosis using noninvasive imaging techniques would markedly enhance early assessment and continuous evaluation of the efficacy of anticancer drugs in a personalized medicinal approach.

The phospholipid bilayer of the cell membrane is made up of four principal phospholipid components: phosphatidylcholine (PC), phosphatidylethanolamine (PE), phosphatidylserine (PS), and sphingomyelin. These four phospholipids are distributed asymmetrically between the two monolayers of the membrane, with PC and sphingomyelin largely populating the extracellular leaflet and PS and PE restricted primarily to the inner leaflet. Breakdown in the maintenance of membrane asymmetry accompanied by prolonged appearance of anionic PS in the outer leaflet of the plasma membrane is a universal indicator of the early and intermediate stages of cell apoptosis.[5,6]

The most common method of detecting PS on a cell surface is to use the protein annexin V, a 36 kDa, Ca^{2+}-dependent PS-binding protein, coupled to a variety of molecular probes (radioactive, optical, or magnetic).[7−11] However, the use of this protein has several disadvantages. It is cleared rapidly from the body with predominantly renal excretion and has a very short blood half-life (<7 min).[12] Given annexin V's high molecular weight and slower diffusion rate as compared with lower molecular weight compounds, there is concern whether optimal imaging of apoptotic cells in solid tumors is achievable with annexin V.[13] Moreover, complete annexin V binding requires up to 1 h and approximately 2.5 mM extracellular Ca^{2+}. This may significantly reduce binding efficacy of annexin V under physiological conditions.

Several alternative approaches have been proposed and evaluated for noninvasive imaging of apoptosis using nanoparticles, proteins, peptides, or low molecular weight compounds that can recognize PS on the surface of apoptotic cells.[14−16] Of these

Received: November 17, 2010
Published: February 24, 2011

peptide-based imaging probes are most attractive because of their low immunogenicity, favorable pharmacokinetic properties, and versatile chemistry, allowing rapid lead compound identification and optimization of stability and affinity. In 1995, Igarashi et al.[17] reported a novel 14-amino-acid consensus sequence shared by protein kinase C and PS decarboxylase thought to be a PS-binding site. A synthetic peptide derived from this sequence, FNFRLKAGQKIRFG (termed first generation PS-binding peptide, or PSBP-0), showed selective binding to PS. However, the binding affinity of PSBP-0 to PS is relatively low, with micromolar affinity based on surface plasmon resonance (SPR) biosensor analysis. We hypothesized that through rational design and screening of targeted peptide libraries, PSBPs with high PS binding affinity in the lower nanomolar range could be identified and used as platforms for the development of noninvasive imaging probes suitable for in vivo optical and nuclear imaging of apoptosis.

When a light beam strikes on a gold film at a specific (resonance) angle, the surface plasmons resonate with light. This phenomenon, termed SPR, is the basis for measuring binding of ligand to receptors on planar gold surfaces. As ligand binds a receptor, an increase in SPR signal [expressed in response units (RUs)] is observed. Advantages of SPR over other biochemical and biophysical techniques include high throughput, direct monitoring of binding without the need for labeling ligands, direct determination of association and dissociation rates, and requirement of small sample volumes.[18−20] To mimic interaction between peptides and membrane lipids within the flow cells, we utilized the L1 chip, which promotes the formation of membrane bilayers with lipophilic anchors covalently linked onto a dextran matrix.[21] In a typical experiment, phospholipids in the form of PS and PC vesicles are immobilized on the flexible dextran matrix of an L1 chip, and peptides flow across the bilayer surface. This high-throughput assay allowed us to rapidly rank the binding of peptides to the PS-coated surface and identify a lead PSBP. We further validated the selective binding of the lead peptide to PS using a combination of enzyme-linked immunosorbent assay (ELISA), fluorescence microscopy, fluorescence-activated cell sorting (FACS), cell uptake of technetium-99 m (^{99m}Tc)-labeled lead peptide, and autoradiography study of tumors in mice treated with taxanes and ^{99m}Tc-labeled lead peptide.

RESULTS AND DISCUSSION

Initial Characterization of a PS-Binding Peptide from PS Decarboxylase. Although limited options are currently available for imaging of apoptosis, they fail to meet the growing demands of biomedical imaging. In this study, we began with a peptide consisting of residues from the PS-binding site of PS decarboxylase, an endogenous protein shown to bind with PS. This 14-mer peptide, FNFRLKAGQKIRFG (termed PSBP-0), was originally identified by a monoclonal antibody designed to bind with PS-binding sites on protein kinase C and PS decarboxylase, an enzyme known to convert PS to PE. The peptide bound with specificity to PS over other lipids, but to our knowledge, no further studies have been published to date.[17] ELISA indicated that PSBP-0 binding to PS was not dependent on calcium and that binding occurred in a dose-dependent manner up to 50 μM, above which the binding was saturated (Figure 1). These promising results prompted us to identify the lead PS-binding peptide with high binding affinity on the basis of FNFRLKAGQKIRFG sequence through high-throughput screening of targeted peptide libraries.

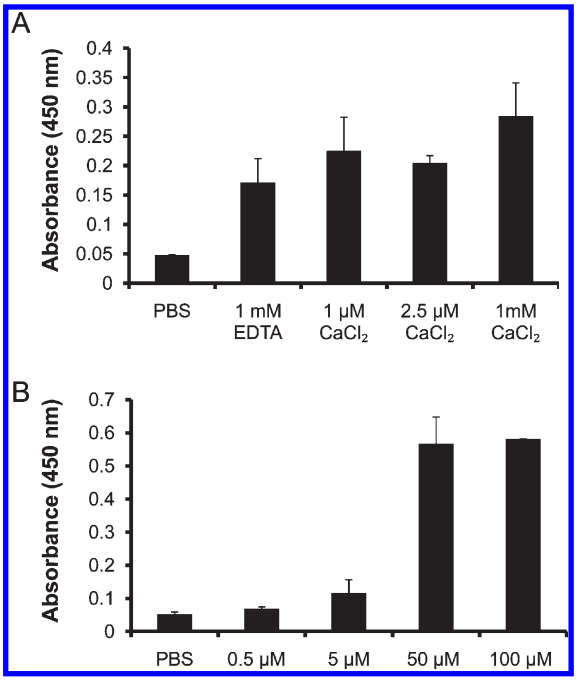

Figure 1. ELISA of PSBP-0 binding to PS. (A) Determination of the role of calcium with biotinylated peptide (5 μM). (B) Dose dependency study (n = 3).

Table 1. Mass Spectral Analysis of Alanine Scanned Peptides

peptides	sequences	M + H or M + 2H (found)	M + H (calculated)
PSBP-0	FNFRLKAGQKIRFG	1680.9236	1680.9814
PSBP-1	FNFRLKAGQKIRF**A**	1694.9665	1694.9971
PSBP-2	FNFRLKAGQKIR**A**G	802.9799	1604.9501
PSBP-3	FNFRLKAGQK**A**FG	798.4621	1591.9174
PSBP-4	FNFRLKAGQ**A**RFG	819.9440	1638.9345
PSBP-5	FNFRLKAGQ**A**IRFG	812.4690	1623.9236
PSBP-6	FNFRLKAG**A**KIRFG	812.4867	1623.9600
PSBP-7	FNFRLK**A**AQKIRFG	848.0060	1694.9971
PSBP-9	FNFRL**A**AGQKIRFG	812.4629	1623.9236
PSBP-10	FNFR**A**KAGQKIRFG	819.9695	1638.9345
PSBP-11	FNF**A**LKAGQKIRFG	798.4628	1595.9174
PSBP-12	FNR**A**LKAGQKIRFG	802.9776	1604.9501
PSBP-13	F**A**FRLKAGQKIRFG	819.4920	1637.9756
PSBP-14	**A**NFRLKAGQKIRFG	802.9940	1604.9501

SPR Screening of PS-Binding Peptides. SPR biosensor technology allows highly sensitive, real-time detection of molecular interactions. The most common types of interactions studied are antigen−antibody and protein−receptor interactions. There has been only limited use of SPR biosensor technology to study the molecular interactions of lipid with peptides.[20,22] Traditionally, determination of kinetic parameters [i.e., association constant (K_a) and dissociation constant (K_d)] has been considered the pinnacle of biosensor experiments. However, much information in addition to K_a and K_d is extractable from SPR sensorgrams. For example, the binding level at the end of the association and dissociation phases reveals details about the binding mechanism, which would not be obtainable from equilibrium-based assays.[23,24]

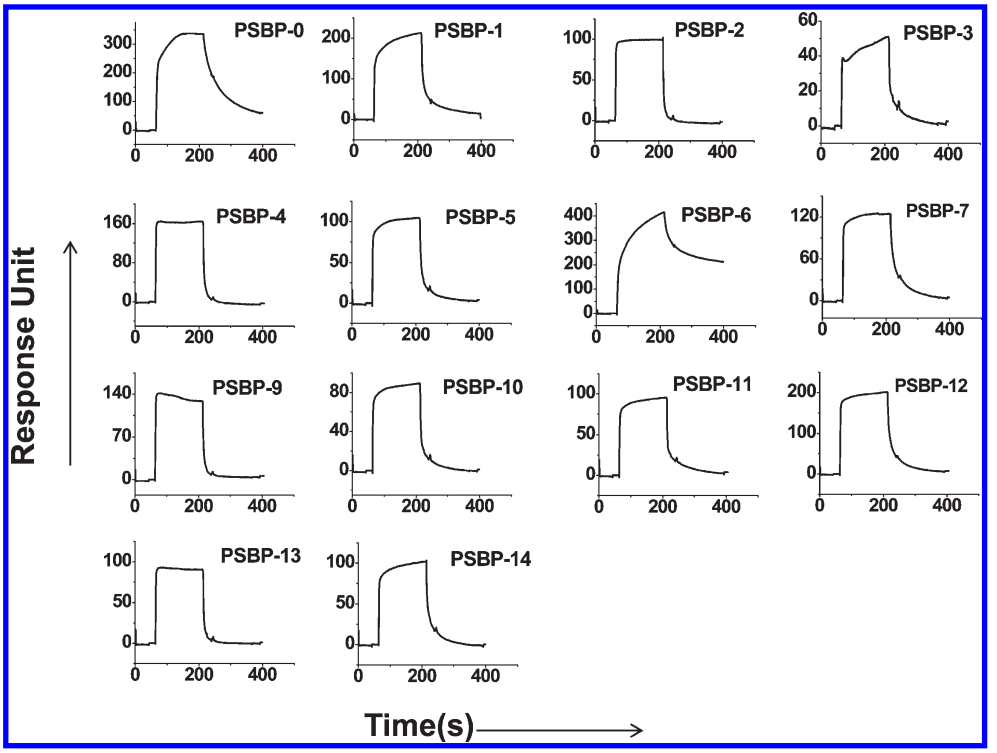

Figure 2. Representative sensorgrams of Ala-scanned peptides used as analytes obtained on PS-coated L1 sensor chip. The specific binding profiles of the peptides to PS were obtained by subtracting from the PS response signal the response signal from the control flow cell coated with PC. The responses are shown in RUs vs time in seconds. The peptide concentration was 10 μM, and the running buffer was HEPES.

In the present study, we used both the binding level at the end of the association phase (binding) and the binding level at the end of the dissociation phase (stability) to rank the peptides. As we were seeking to identify PSBPs to be developed as imaging probes, the stability of the complex formed between the lead PSBP and the PS was an important feature because it dictates the contrast between the target cells and the background after the imaging probe has cleared from the normal tissues. The PS-specific binding profiles of the PSBPs to the immobilized PS bilayer were obtained by subtracting the response signal from the PC-coated control flow cell from the PS response signal. PC was used as a control because it is one of the most abundant lipids in the outer cell membrane. PSBP-0 was included with each run, and the results were normalized to the average PSBP-0 value to account for variability in chip coating in different runs.

To identify amino acid residues that contribute to PS affinity, each of the 14 residues of PSBP-0 except the endogenous alanine residue at position 8 (Ala^8) was replaced with Ala (Table 1), and the 13 resulting peptides were ranked on the basis of the association and dissociation binding levels in SPR sensorgrams. The effect of an Ala substitution was highly dependent on the replaced residue's relative contribution to the binding energy and interaction with the neighboring residues. The individual sensorgrams in Figure 2 and summary of normalized binding levels in Figure 3A show that all of the 13 Ala-substituted peptides except PSBP-6 had lower affinity for PS than the parent PSBP-0 peptide. In addition, all of the 13 Ala-substituted peptides except PSBP-6 were characterized by fast and nearly complete dissociation. These findings indicated that amino acids in 12 of 13 positions contributed to the PS binding at both the association and the dissociation phases. Interestingly, substitution of Arg^3 with Ala (PSBP-3) resulted in the lowest binding level and stability. This suggests that the positively charged Arg^3 plays an important role in the interaction between the PS and the peptide.

Significantly, PSBP-6 (molecular mass = 1623 Da), where Gln^6 is replaced by Ala, showed the highest relative binding level and stability and had levels surpassing those of the first generation PSBP-0 (Figure 3A). This finding indicates that Gln^6 is not critical for the binding of PSBP-0 to PS and that the binding profile may be enhanced by optimization at this residue. It may be that substitution of Gln^6 with Ala reduces the steric hindrance and/or polarity, allowing the peptide to bind to the lipid membrane more favorably.

Next, a peptide library based on PSBP-6 in which the Ala^6 residue was replaced with each of the 20 amino acids was synthesized and evaluated (Table 2). Binding profiles of the 20 peptides were ranked as shown in Figure 3B. As previously done, binding values of PC were subtracted from binding values of PS to yield specific PS binding. Although many of the modified peptides bound with higher affinity than the starting peptide (PSBP-0), only three (those in which Ala^6 was replaced with Val, Thr, or Cys) showed binding levels similar to those of PSBP-6. In general, substitution with hydrophobic amino acids (Val, Thr, Ile, Tyr, Phe, etc.) preserved the binding affinity to PS, whereas substitution with hydrophilic amino acids (Glu, Asp, Ser, etc.) reduced the binding affinity to PS. As expected, the introduction of negatively charged amino acids significantly decreased affinity for PS, but the introduction of positively charged amino acids did not appear to significantly increase affinity for PS. On the basis of these results, PSBP-6 remained as the lead compound.

Lastly, Lys[di(2-pyridinemethyl)]-CO_2H, termed a single amino acid chelator (SAAC), was introduced at specific positions of PSBP-0 and PSBP-6 for several reasons (Table 3). First, SAAC can form a stable complex with ^{99m}Tc, the most extensively used

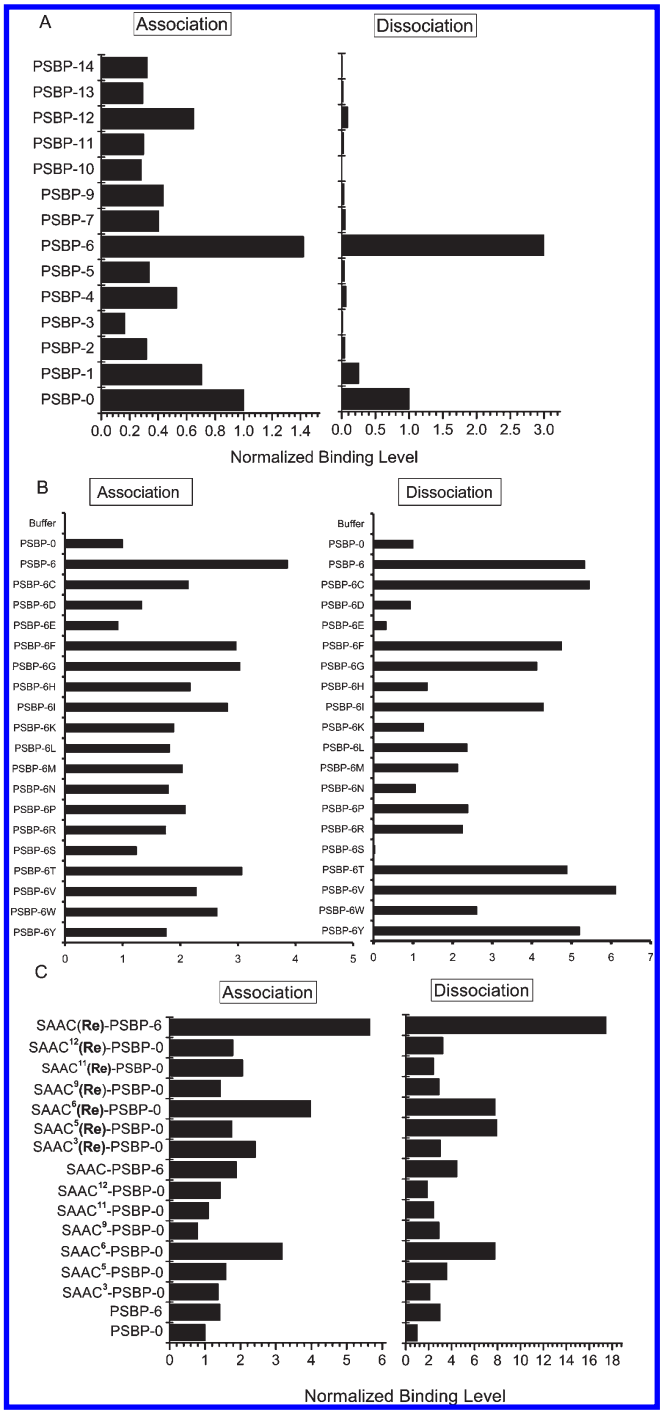

Figure 3. Summary of binding level at the end of association and dissociation phases for (A) Ala-scanned peptides, (B) peptides derived from PSBP-6 having Ala[6] substituted with different amino acids, and (C) peptides containing SAAC and SAAC-Re. The specific binding profiles of the peptides to the immobilized PS were obtained by subtracting from the PS response signal the response signal from the control flow cell coated with PC. Binding levels were normalized to that of PSBP-0 (RUs = 1.0), which was run in parallel for every experiment.

radiometal in nuclear medicine.[25−27] Second, SAAC can also form a stable complex with rhenium (Re).[28,29] This complex has physical and biodistribution properties similar to those of ^{99m}Tc and is often used as a nonradioactive alternative to ^{99m}Tc for structural characterization and in vitro evaluation.[30] Third, SAAC

Table 2. Mass Spectral Analysis of Peptides with Gln[6] in PSBP-0 Substituted with Selected Amino Acids

peptides	sequences	M + 2H (found)	M + H (calculated)
PSBP-0	FNFRLKAG**Q**KIRFG	840.8661	1680.9814
PSBP-6	FNFRLKAG**A**KIRFG	812.5027	1623.9600
PSBP-6C	FNFRLKAG**C**KIRFG	828.4785	1655.9082
PSBP-6D	FNFRLKAG**D**KIRFG	834.5106	1667.9259
PSBP-6E	FNFRLKAG**E**KIRFG	841.4915	1681.9415
PSBP-6F	FNFRLKAG**F**KIRFG	850.5029	1699.9674
PSBP-6G	FNFRLKAG**G**KIRFG	805.3307	1609.9204
PSBP-6H	FNFRLKAG**H**KIRFG	845.5011	1689.9579
PSBP-6I	FNFRLKAG**I**KIRFG	833.5238	1665.9830
PSBP-6K	FNFRLKAG**K**KIRFG	841.0192	1680.9939
PSBP-6L	FNFRLKAG**L**KIRFG	833.5121	1665.9830
PSBP-6M	FNFRLKAG**M**KIRFG	842.9900	1683.9395
PSBP-6N	FNFRLKAG**N**KIRFG	833.9906	1666.9419
PSBP-6P	FNFRLKAG**P**KIRFG	825.5009	1649.9517
PSBP-6R	FNFRLKAG**R**KIRFG	855.5158	1709.0001
PSBP-6S	FNFRLKAG**S**KIRFG	820.5013	1639.9310
PSBP-6T	FNFRLKAG**T**KIRFG	827.3136	1653.9466
PSBP-6 V	FNFRLKAG**V**KIRFG	826.5162	1651.9674
PSBP-6W	FNFRLKAG**W**KIRFG	870.5102	1738.9783
PSBP-6Y	FNFRLKAG**Y**KIRFG	858.4989	1715.9623

is a lipophilic chelating group (bispyridine) and, after chelation with radiometal ions, forms SAAC(^{99m}Tc) and SAAC(Re) complexes; the resulting positively charged hydrophobic species are expected to have enhanced interaction with negatively charged PS.

We substituted Gln[6] and Arg[3] in PSBP-0 with SAAC because in our SPR assay, substitution of Gln[6] and Arg[3] with Ala yielded peptides with markedly increased PS binding levels (PSBP-6) and markedly reduced PS binding levels (PSBP-3), respectively. In addition, Lys[5], Lys[9], Arg[11], and Phe[12] in PSBP-0 were replaced with SAAC. These amino acids are either positively charged or hydrophobic and are thought to contribute significantly to the interaction between PSBP-0 and negatively charged PS lipid. We hypothesized that replacing these amino acids with more hydrophobic and more strongly positively charged SAAC(Re) and SAAC(^{99m}Tc) would enhance the binding interaction between PSBP peptides and PS. Finally, SAAC was introduced to the N terminus of the lead compound, PSBP-6, to give SAAC-PSBP-6 (Table 3).

The SPR ranking data according to the association and dissociation binding levels of these SAAC derivatives and their corresponding Re chelates are summarized in Figure 3C. As compared to PSBP-6, the peptide having SAAC introduced at the N terminus of PSBP-6 (SAAC-PSBP-6) and peptides having the Lys[5] or Gln[6] residues in PSBP-0 substituted with SAAC showed increased binding to PS. Both Ala substitution data (Figure 3A) and SAAC substitution data (Figure 3C) support the notion that manipulation of Gln[6] contributed significantly to enhanced peptide−PS lipid interaction. In general, chelation with Re increased the binding affinity of PSBP peptides as compared to their corresponding nonchelated peptides because of the positive charge of the metal complexes (Figure 3C). In particular, SAAC[6](Re)-PSBP-0 and SAAC(Re)-PSBP-6 showed the highest association and dissociation binding levels. The SPR sensorgrams

Table 3. Mass Spectra Analysis of SAAC Scanned Peptides

peptides	sequences	M + H or M + 2H (found)	M + H (calculated)
SAAC^{3}-PSBP-0	FNFRLKAGQKI(**SAAC**)FG	918.0298	1835.0597
SAAC^{5}-PSBP-0	FNFRLKAGQ(**SAAC**)IRFG	932.0150	1863.0658
SAAC^{6}-PSBP-0	FNFRLKAG(**SAAC**)KIRFG	932.0726	1863.1022
SAAC^{9}-PSBP-0	FNFRL(**SAAC**)AGQKIRFG	1863.0578	1863.0658
SAAC^{11}-PSBP-0	FNF(**SAAC**)LKAGQKIRFG	918.0463	1835.0597
SAAC^{12}-PSBP-0	FN(**SAAC**)RLKAGQKIRFG	1830.0665	1830.0665
SAAC-PSBP-6	(**SAAC**)FNFRLKAGAKIRFG	932.0150	1943.1393
SAAC^{3}(Re)-PSBP-0	FNFRLKAGQKI(**SAACRe**$^{+}$))FG	1053.0200	2104.9924
SAAC^{5}(Re)-PSBP-0	FNFRLKAGQ(**SAAC**(**Re**$^{+}$))IRFG	1067.0187	2132.9985
SAAC^{6}(Re)-PSBP-0	FNFRLKAG(**SAAC**(**Re**$^{+}$))KIRFG	1067.0394	2133.0349
SAAC^{9}(Re)-PSBP-0	FNFRL(**SAAC**(**Re**$^{+}$))AGQKIRFG	2132.9976	2132.9985
SAAC^{11}(Re)-PSBP-0	FNF(**SAAC**(**Re**$^{+}$))LKAGQKIRFG	1053.0223	2104.9924
SAAC^{12}−Re-PSBP-0	FN(**SAAC**(**Re**$^{+}$))RLKAGQKIRFG	2100.0073	2100.0094
SAAC(Re)-PSBP-6	(**SAAC**(**Re**$^{+}$))FNFRLKAGQKIRFG	1102.5719	2205.0798

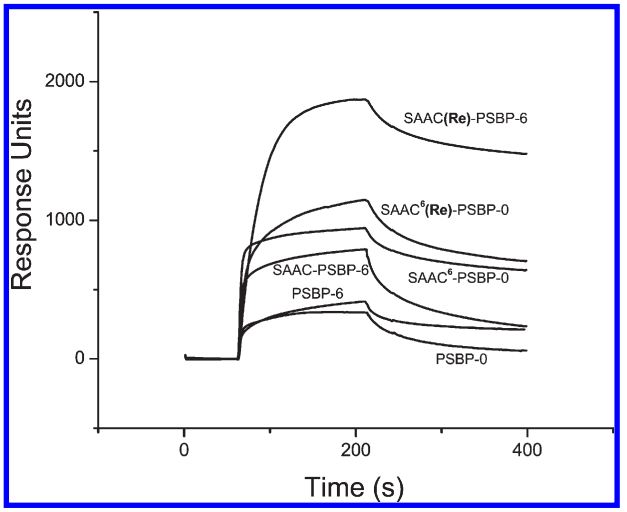

Figure 4. Sensorgrams for five lead PSBP peptides and the original peptide (PSBP-0). An L1 sensor chip was coated with PS. The specific binding profile of each peptide (10 μM) to immobilized PS was obtained by subtracting from the PS response signal the response signal generated from the control flow cell with sensor chip coated with PC. The responses are shown in RUs vs time in seconds. The running buffer was HEPES.

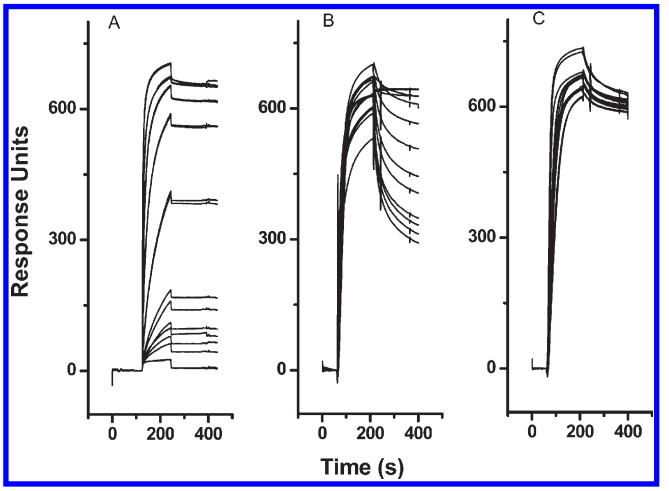

Figure 5. Inhibition of annexin V's binding to PS-coated L1 chip by SAAC-PSBP-6. (A) Effect of annexin V concentration on response. Sensorgrams were obtained at concentrations of annexin V ranging from 2 to 256 nM in a 2-fold dilution series in the presence of 3 mM $CaCl_2$. (B) Inhibition of annexin V binding by SAAC-PSBP-6. Sensorgrams were obtained with mixtures of annexin V (100 nM) and increasing concentrations of SAAC-PSBP-6 (2−256 nM in a 2-fold dilution series). (C) Sensorgrams were obtained with mixtures of annexin V (100 nM) and increasing concentrations of scrambled peptide (2−256 nM in a 2-fold dilution series).

comparing the PS binding affinity of SAAC^{6}(Re)-PSBP-0 and SAAC(Re)-PSBP-6 and their corresponding nonchelated peptides are presented in Figure 4. These data clearly show that the peptide with Re chelated to SAAC-PSBP-6 exhibited much greater PS binding than the peptide with Re chelated SAAC^{6}-PSBP-0. The dissociation constants, K_d, calculated after fitting the SPR data set to 1:1 mass transfer model were 1.38×10^{-6}, 1.0×10^{-7}, and 2.59×10^{-8} M for PSBP-0, PSBP-6, and SAAC(Re)-PSBP-6, respectively.

Binding of Annexin V to PS Was Blocked by SAAC-PSBP-6. In an SPR assay, binding to macromolecules yields a much greater signal than binding to low molecular weight analytes. We directly monitored changes in annexin V binding to PS-coated L1 sensor chips. Increasing the concentration of annexin V from 2 to 256 nM caused a substantial increase in responses, plateauing by 256 nM (Figure 5A). In competition experiments, 100 nM annexin V (~36 kDa) was mixed with increasing concentrations of either SAAC-PSBP-6 (~2 kDa) or a scrambled PSBP-0 peptide (KFFAILNGRQGKFR). The mixtures were then injected into the SPR system. The resulting sensorgrams showed decreased binding of annexin V to PS with increasing concentrations of SAAC-PSBP-6. At a SAAC-PSBP-6 concentration of 256 nM, the response attributed to annexin V's binding to PS was reduced to ~50% of the original level (Figure 5B). In contrast, less than 5% of bound annexin V was stripped away from the chip surface by the scrambled peptide at 256 nM (Figure 5C). Further SPR studies showed no significant difference in SAAC(Re)-PSBP-6 response levels in the presence or absence of Ca^{2+} (data not shown). These results indicate that SAAC-PSBP-6 and annexin V likely compete for the same binding site. However, unlike annexin V, the binding of SAAC-PSBP-6 to PS is independent of Ca^{2+}.

SAAC(^{99m}Tc)-PSBP-6 Selectively Binds to Apoptotic Cells. We next labeled SAAC-PSBP-6, the peptide with the highest

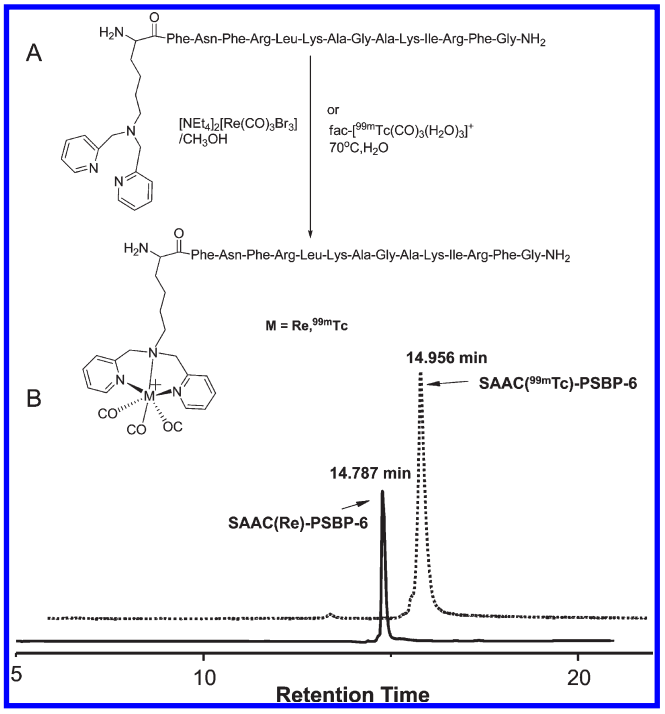

Figure 6. (A) Reaction scheme of conjugation of peptide SAAC-PSBP-6 with Re and ^{99m}Tc. (B) Comparison of chromatograms between SAAC(Re)-PSBP-6 and SAAC-(^{99m}Tc)-PSBP-6 obtained under the same chromatographic conditions (solvent A, 0.1% TFA in water; solvent B, acetonitrile; gradient, 0−90% B in A over 25 min; flow rate, 1.0 mL/min; C18 4.6 mm × 250 mm, 5 μm column). Rechelate was detected with an ultraviolet light detector; ^{99m}Tc-chelate was detected with an NaI crystal radiodetector.

binding level to PS upon Re chelation, with ^{99m}Tc. Figure 6A shows the reaction scheme for the synthesis of SAAC(^{99m}Tc)-PSBP-6 and nonradioactive SAAC(Re)-PSBP-6. The structure of SAAC(Re)-PSBP-6 was confirmed by mass spectroscopy, which revealed a m/e value of 1102.5719 corresponding to the $(M + Re + H)^{2+}$ peak (calcd $C_{98}H_{145}N_{28}O_{19}Re$, 1102.5399) by high-resolution electrospray ionization mass spectrometry (HRMS-ESI). High-performance liquid chromatography (HPLC) analysis revealed that SAAC(^{99m}Tc)-PSBP-6 had a retention time of 14.96 min, which was almost identical to that of Re-chelated SAAC-(Re)-PSBP-6 (retention time = 14.79 min), indicating that SAAC(^{99m}Tc)-PSBP-6 had the same structure as SAAC(Re)-PSBP-6 (Figure 6B). The radiolabeling efficiency and specific activity were >95% and 0.2 mCi/μg, respectively. The stability of SAAC(^{99m}Tc)-PSBP-6 was evaluated using a ligand challenge method,[29] in which a large excess of cysteine and histidine was used to test the complex's tendency to undergo transchelation. No transchelation was observed after the radiotracer was incubated at 37 °C for up to 5 h, indicating that SAAC(^{99m}Tc)-PSBP-6 was stable up to 5 h.

Previous studies have shown that tumor necrosis factor-related apoptosis-inducing ligand (TRAIL) induces apoptosis in a time- and dose-dependent manner.[31] When SAAC(^{99m}Tc)-PSBP-6 was incubated with DLD1 human colon carcinoma cells pretreated with increasing doses of TRAIL, increasing amounts of the peptide radiotracer were bound to the treated cells. Minimal SAAC(^{99m}Tc)-PSBP-6 was found associated with the untreated viable cells (Figure 7A). These results confirm that SAAC(^{99m}Tc)-PSBP-6 selectively binds to apoptotic cells.

Imaging Apoptotic Cells in Vitro with 5-Carboxyfluorescein (FAM)-SAAC(Re)-PSBP-6. To quantify SAAC(Re)-PSBP-6 binding to apoptotic cells, we labeled SAAC(Re)-PSBP-6 and its corresponding scrambled peptide (KFFAILNGRQGKFR) with FAM. Both compounds were incubated with either viable DLD1 cells or apoptotic DLD1 cells that had been treated with TRAIL for 2 h at 37 °C. Figure 7B shows results from quantitative FACS analysis. Binding of FAM-SAAC(Re)-PSBP-6 was observed in 62% of TRAIL-treated cells but only 18% of nontreated viable cells. Moreover, when TRAIL-treated cells were coincubated with cold annexin V and FAM-SAAC(Re)-PSBP-6, annexin V was able to compete for PS, resulting in a 65% drop in FAM-SAAC(Re)-PSBP-6 binding to apoptotic cells (Figure 7B). These results indicate that FAM-SAAC(Re)-PSBP-6 is a selective marker for apoptotic cells and that annexin V and FAM-SAAC(Re)-PSBP-6 share the same binding space on the membrane of apoptotic cells.

The ability of SAAC(Re)-PSBP-6 to distinguish between apoptotic and viable cells was further assessed via fluorescence microscopy (Figure 7C). TRAIL-induced apoptotic response was visualized by staining of TRAIL-treated DLD1 cells with Alexa Fluor 594−annexin V. These cells were readily labeled with FAM-SAAC(Re)-PSBP-6 but not with FAM-labeled scrambled peptide. FAM-SAAC(Re)-PSBP-6 (green) colocalized with Alexa Fluor 594−annexin V (red), suggesting specific binding of FAM-SAAC(Re)-PSBP-6 to PS on the cell membrane. Neither annexin V nor FAM-SAAC(Re)-PSBP-6 stained viable cell membrane (Figure 7C). In conclusion, imaging of apoptotic cells is feasible in vitro with fluorescently labeled SAAC(Re)-PSBP-6.

Biodistribution. SAAC(^{99m}Tc)-PSBP-6 displayed significantly higher uptake in B16/F10 tumors treated with poly(L-glutamic acid)-paclitaxel (PG-TXL) (4.06 ± 0.55% ID/g) than did in the nontreated tumors (1.61 ± 0.33% ID/g) ($P < 0.001$) (Figure 8). The biodistribution data show that the liver and the kidney were the major organs taken up SAAC(^{99m}Tc)-PSBP-6.

Treatment with PG-TXL induced extensive apoptotic response at 24 h (compare Figure 9A,B, right panel), which was confirmed by terminal deoxynucleotidyl transferase-mediated dUTP nick end labeling (TUNEL) staining. Autoradiography shows that the intratumoral distribution of radioactivity correlated well with the tumor apoptosis (Figure 9). These results indicate that uptake of SAAC-(^{99m}Tc)-PSBP-6 in tumors of taxane-treated mice is mediated through binding of the radiotracer to apoptotic cells.

It should be pointed out that PS externalization during the cell death is by no means an exclusive apoptotic event. Previous studies have revealed that autophage, early necrosis, and mitotic catastrophe are all associated with active presentation of PS at the cell membrane.[32] Thus, SAAC(^{99m}Tc)-PSBP-6 is likely suitable for imaging various events leading to apoptosis and other forms of cell death. Further work in appropriate preclinical models of cell death and apoptosis is needed to define the sensitivity and specificity of this new PS-targeted imaging agent.

CONCLUSIONS

Through logical screening of targeted peptide libraries against immobilized PS using SPR sensor technology, we identified a 14-mer peptide, SAAC(Re/^{99m}Tc)-PSBP-6, which demonstrated nanomolar binding affinity to PS. The introduction of the hydrophobic and cationic SAAC to the peptide not only enhanced the binding affinity of the peptide but also allowed high-efficiency labeling of the peptide with ^{99m}Tc, a γ-emitting

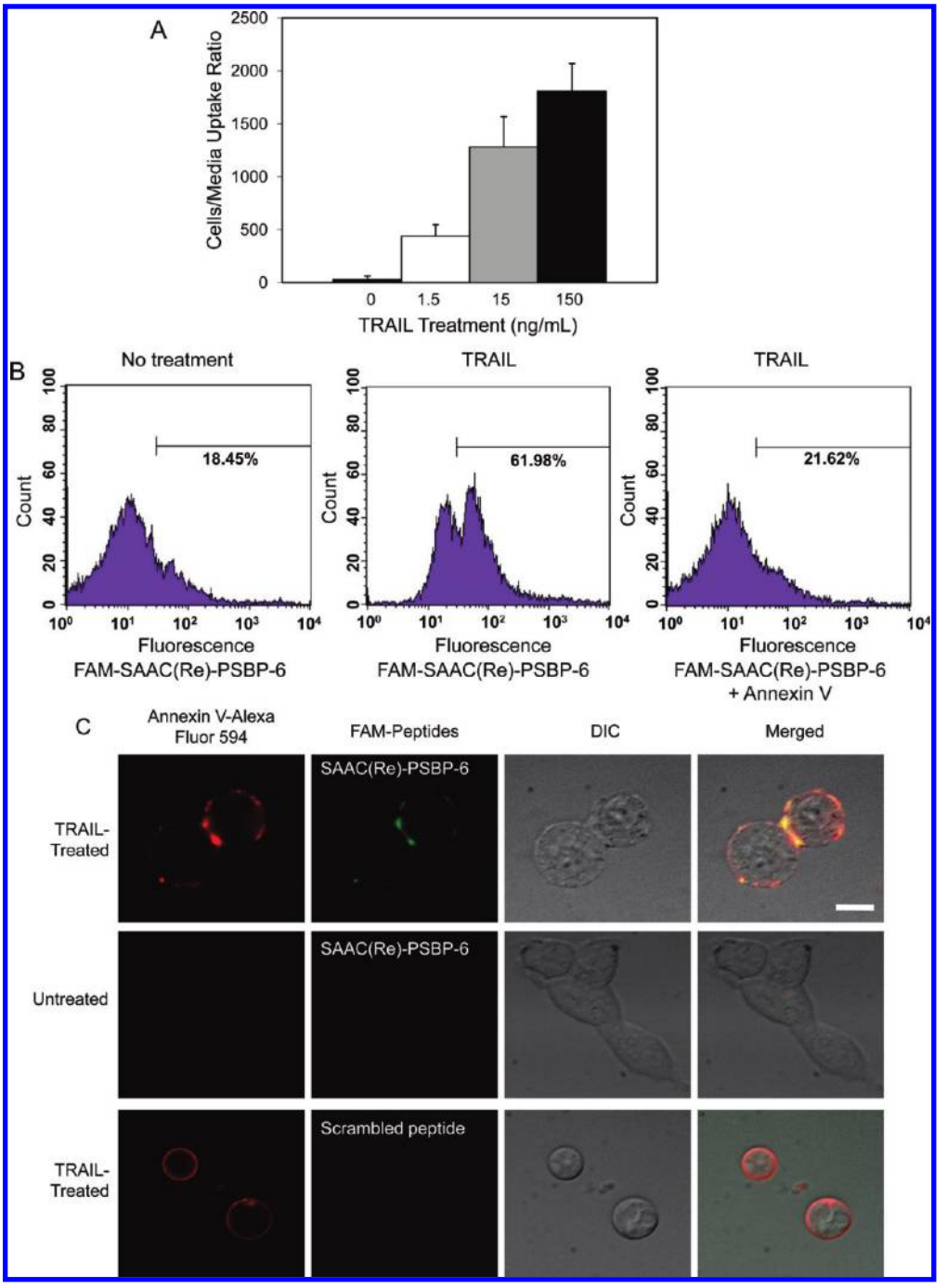

Figure 7. Uptake of radiolabeled and fluorescent-labeled SAAC-PSBP-6 peptide in apoptotic cells. The cell-to-medium uptake ratio is expressed as [cpm/μg protein in pellet]/[cpm/μg medium]. (A) SAAC($^{99\,m}$Tc)-PSBP-6 exhibited increased uptake in apoptotic DLD1 cells in vitro in response to increasing dose of TRAIL. (B) FACS analysis of DLD1 cells. Cells were treated with FAM-SAAC(Re)-PSBP-6 (20 μM) only (left), TRAIL at 150 ng/mL for 3 h followed by FAM-SAAC(Re)-PSBP-6 (middle), or TRAIL followed by FAM-SAAC(Re)-PSBP-6 and annexin V (5 μM) (right). The percentage of cells with FAM fluorescent signal over the gate is shown. Annexin V inhibited binding of FAM-SAAC(Re)-PSBP-6 to apoptotic cells. (C) FAM-SAAC(Re)-PSBP-6 colocalized with annexin V in apoptotic cells. Fluorescence microphotographs were acquired with TRAIL-treated DLD1 cells or untreated control cells after coincubation with Alexa Fluor 594-annexin V (red) and FAM-SAAC(Re)-PSBP-6 (green). TRAIL-treated cells were stained by both annexin V and FAM-SAAC(Re)-PSBP-6 (top row). FAM-scrambled peptide did not bind with apoptotic cells (middle row), and viable cells were not stained with either annexin V or FAM-SAAC(Re)-PSBP-6 (bottom row). Scale bar, 20 μm.

radionuclide routinely used clinically in nuclear medicine. Selective binding to apoptotic cells by radiolabeled SAAC(^{99m}Tc)-PSBP-6 and fluorescence-labeled SAAC(Re)-PSBP-6 was confirmed using a combination of SPR, fluorescence microscopy, FACS, and radiotracer uptake techniques of ^{99m}Tc-labeled peptide. In vivo evaluation of biodistribution, histology, and autoradiography of tumors in mice treated with a taxane derivative PG-TXL confirmed that SAAC(^{99m}Tc)-PSBP-6 has high binding affinity to apoptotic tumors and is suitable for imaging therapy-induced apoptosis and/or cell death. Further studies—including

improvement in pharmacokinetic properties and imaging with other cell death modes—are needed to develop an optimal peptide-based imaging agent suitable for in vivo imaging of apoptosis.

EXPERIMENTAL SECTION

Materials and Methods. *Materials.* All amino acid derivatives were purchased from Novabiochem (San Diego, CA), Bachem (Torrance, CA), and Chem-Impex International (Wood Dale, IL). 5-Carboxyl fluorescein (FAM) and D-biotin were purchased from Sigma-Aldrich (St. Louis, MO). Fmoc-Lys[di(2-pyridinemethyl)]-CO_2H (SAAC) was synthesized according to Levadala et al.[28] The organometallic precursor $(NEt_4)_2[Re(CO)_3Br_3]$ was synthesized according to previously published procedures.[33] 1,2-Dioleoyl-*sn*-glycero-3-[phospho-L-serine, PS] and 1,2-dioleoyl-*sn*-glycero-*sn*-[phosphocholine, PC] were purchased from Avanti Polar Lipids (Alabaster, AL). Reagent grade solvents were used without further purification unless otherwise specified. Recombinant human TRAIL was purchased from Millipore (Billerica, MA). Alexa Fluor 594—annexin V conjugate, fetal bovine serum, and RPMI-1640 culture medium were purchased from Invitrogen (Carlsbad, CA). The protein assay kit was obtained from Bio-Rad Laboratories (Hercules, CA). Isolink carbonyl reaction kit for ^{99m}Tc labeling was a gift from Mallinckrodt (St. Louis, MO).

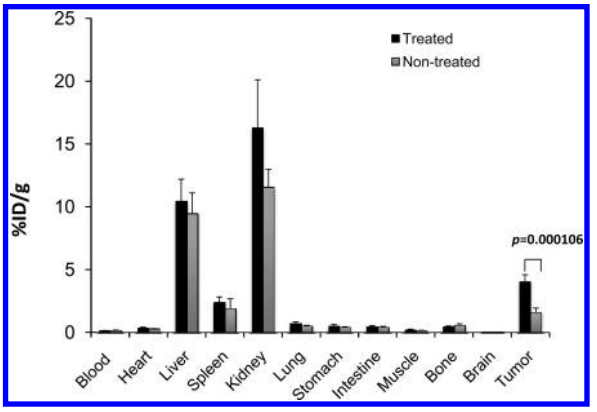

Figure 8. Biodistribution of SAAC($^{99\ m}$Tc)-PSBP-6 at 4 h after injection in mice with B16/F10 tumors. The mice were either untreated (n = 4) or treated with PG-TXL (n = 5) 24 h prior to radiotracer injection. The data represent means ± standard deviations.

General Procedure for Peptide Synthesis. Solid-phase syntheses were carried out on a Prelude automatic peptide synthesizer (PTI, Tucson, AZ) using commercially available Rink resin. The resins (0.05−0.1 g) were swollen and washed five times each with 1.5 mL of DMF/CH_2Cl_2. Fmoc groups were removed with 3 × 1.5 mL of 20% piperidine/DMF for 5 min each. For coupling, 3-fold excesses of Fmoc-amino acids, diisopropylcarbodiimide, and 1-hydroxybenzotriazole (HOBt) were used in 3 mL of DMF/CH_2Cl_2. This coupling procedure was then repeated. After deprotection and coupling steps, resins were washed three times each with 3 mL of DMF/CH_2Cl_2. Upon completion of the peptide chain elongation, resins were washed three times each with 3 mL of CH_2Cl_2 and were treated with trifluoroacetic acid (TFA):triisopropylsilane: H_2O (95:2.5:2.5) three times for 15 min each. The combined filtrates were left at room temperature for 1−2 h, and the volumes were reduced in vacuum. Peptides were precipitated in ice-cold ethyl ether, collected by centrifugation, and washed two times with ethyl ether and centrifuged. After they were dried, peptides were purified by reverse-phase HPLC on an Agilent 1200 system (C-18, Vydac, 10 mm × 250 mm, 10 μm). Gradients of acetonitrile in H_2O [containing 0.1% TFA or acetonitrile in 0.01 M NH_4OAc (pH 6.5)] were run at 10 mL/min. Peptides were lyophilized and dried in vacuum over P_2O_5 at room temperature for 24 h prior to use. The purity of peptides was verified by

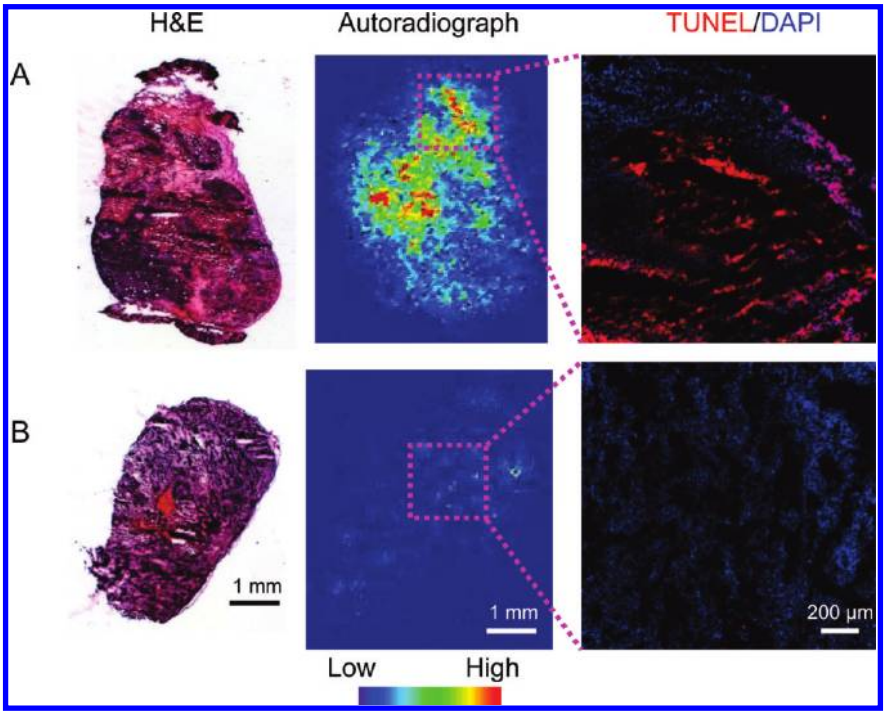

Figure 9. Representative autoradiographs and fluorescence microphotographs of tumor sections stained with TUNEL 4 h following intravenous injection of SAAC($^{99\ m}$Tc)-PSBP-6 in nude mice bearing B16/F10 tumors. (A) Mouse was treated with PG-TXL (100 mg equivalent paclitaxel/kg) to induce apoptosis. (B) Nontreated mouse. Red in fluorescent microphotographs shows TUNEL-positive apoptotic cells; blue represents DAPI-stained cells.

reverse-phase HPLC on an Agilent LC-MSD-TOF system (Santa Clara, CA). A Vydac 4.6 mm × 150 mm C18 peptide/protein column or a Phenomenex Luna 4.6 mm × 250 mm C18 column was employed in the HPLC system using two mobile systems, one with a gradient of acetonitrile in H_2O with 0.1% TFA and the other with a gradient of acetonitrile in 0.01 M NH_4OAc (pH 6.5). Gradients were 0−80% acetonitrile over a period of 30 min in both systems. HRMS-ESI acquired in the positive ion mode was used to identify the peptides. In all cases, the peptides were more than 95% pure. The peptide sequences and their characterization by HRMS-ESI are summarized in Tables 1−3.

Conjugation of Peptide with Re and ^{99m}Tc. The Re complex was prepared in quantitative yield by adding a stoichiometric amount of $(NEt_4)_2[Re(CO)_3Br_3]$ in methanol to an aqueous solution of SAAC-containing peptides. The products were characterized by high-resolution liquid chromatography−mass spectrometry. $[^{99m}Tc(CO)_3(H_2O)_3]^+$ was prepared using the following general procedure: 1.0 mL of $^{99m}TcO_4^-$ (2−5 mCi) was added to an Isolink carbonyl kit vial. The solution was heated in an oil bath at 100 °C for 20 min. The solution was then cooled for 5 min and vented. One hundred twenty microliters of 1 N HCl was added to adjust the pH to 6−7 and to decompose any residual boranocarbonate. ^{99m}Tc-$(CO)_3(H_2O)_3$ (0.5 mL, 2 mCi) was added to a sealed vial containing 10−20 μg of SAAC-containing peptide in distilled water. The vial was heated for 30 min at 75 °C. After the sample was cooled, the complexes were characterized using HPLC.

Conjugation of Peptide with FAM or Biotin. FAM or biotin was introduced at the N-terminal of the peptide sequence while it was still attached to the solid phase. For coupling, 3-fold excess of FAM or D-biotin, diisopropylcarbodiimide, and HOBt were used, and the reaction was allowed to proceed until resin samples tested negative with ninhydrin tests. On completion of the reaction, the fluorescent FAM-labeled peptides and biotinylated peptide were cleaved from resin and purified by HPLC as described in the preceding paragraph. FAM-SAAC(Re)-PSBP-6 was found to have a *m*/*e* value of 1281.5752 $(M + Re + H)^{2+}$ (calcd $C_{119}H_{155}N_{28}O_{25}Re$, 1281.5638) by HRMS-ESI.

Stability of ^{99m}Tc Complex. Aliquots of 30 μL of ^{99m}Tc complex were added to 270 μL of 0.01 M cysteine or 0.01 M histidine solution in phosphate-buffered saline (PBS). The samples were incubated at 37 °C and analyzed by HPLC after 1 and 5 h to verify stability.

ELISA. Ninety-six-well cell suspension plates (Cell Star, Greiner Bio-One, Monroe, NC) were washed for 15 min with 1-butanol and twice for 5 min each with ethanol. The plates were coated with PS or PC, which were dissolved for a final concentration of 6 μg/mL in ethanol and distributed at 0.3 μg/well in the plate. The lipids were dried overnight at room temperature under a ventilation hood, and the plate was washed three times with PBS (pH 7.4) to remove any nonbinding lipids. Next, 200 μL of blocking solution (3% bovine serum albumin in PBS) was added to each well, and the plates were incubated at room temperature for 1 h on a shaker to block nonspecific binding. Wells were washed twice for 5 min with PBS, 200 μL of biotinylated peptide was added, and plates were incubated for 30 min on a shaker. Following several washes with PBS, plates were developed with a Vectastain ABC kit (Vector Laboratories, Inc., Burlingame, CA), where the developing solutions were incubated for 30 min at room temperature and then washed eight times with PBS containing 0.1% Tween-20. The addition of tetramethylbenzidine substrate produced a bluish product, at which time 100 μL/well of 2 M HCl was added to neutralize the reaction. A standard 96-well plate reader was used to measure absorbance at 450 nm, and wells with lipid + PBS or lipid +50 μM D-biotin were used as background controls. Annexin V (Biovision, Mountain View, CA) and anti-PS antibodies (Millipore, Billerica, MA) were used to validate relative PS coating levels.

Preparation of Small Unilamellar Vesicles. Small unilamellar vesicles were prepared as described previously.[8] Briefly, rotary evaporation under reduced pressure of the chloroform phospholipid stock solution resulted in a thin lipid film on the sides of a round-bottom flask. The lipid films were thoroughly dried to remove residual organic solvent by rotation under vacuum for 2 h. Hydration of each lipid film was achieved by addition of 10 mM HEPES buffer (pH 7.4) containing 2.5 mM $CaCl_2$ and 100 mM NaCl to give a final 5 mM concentration of phospholipid vesicles. This suspension was then thoroughly mixed for 2 h on a rotary evaporation system without vacuum. The resultant hydrated vesicles were then stored on dry ice overnight. Prior to loading to the L1 chip surface, the vesicles were extruded 20 times through a 50 nm polycarbonate filter using an extrusion apparatus to give small unilamellar vesicles composed of only PS or PC. The L1 surfaces were coated with vesicles by injecting 20 μL of 5 mM phospholipid vesicle suspension at a rate of 5 μL/min for 20 min.

SPR Measurements. A Biacore 3000 apparatus (Biacore Life Sciences, Uppsala, Sweden) equipped with a precoated L1 chip was used for SPR measurements using 10 mM HEPES (pH 7.4, 100 mM NaCl) with or without 2.5 mM $CaCl_2$ as the running buffer. The buffer solution was filtered through a 0.22 μm filter and degassed thoroughly. The solutions of peptides or human recombinant annexin V of various concentrations in the running buffer were injected over the flow cells at a flow rate of 20 μL/min for predetermined time periods. The peptide solution was then replaced with the running buffer to allow the peptide to dissociate. RU binding levels were recorded for all injections before and after the onset of dissociation.The specific binding profiles of the peptides to the immobilized PS were obtained after subtracting from the PS response signal the response signal from the control flow cell (PC). A sensorgram was obtained by plotting the SPR RU against time. An increase in RU from the injection point and a decrease in RU from the beginning of the washing step as measures of association and dissociation, respectively, were determined and used to rank the relative peptide binding affinities. Following each injection/dissociation cycle, the flow cell surfaces were regenerated by injection of by injection of 10 mM glycine solution (pH 3.0).

Cell Binding. DLD1 human colon carcinoma cells were obtained from the American Type Culture Collection (Manassas, VA). The cells were grown in 6 cm cell culture dishes to subconfluent densities in Dulbecco's modified Eagle's medium/F12 culture medium containing 10% fetal bovine serum. Apoptosis was induced by treating cells with TRAIL (100 μL and 1.5, 15, or 150 ng/mL) for 2 h at 37 °C. The media were replaced with 2 mL of media containing SAAC(^{99m}Tc)-PSBP-6 (∼40 μCi/mL, 50 μg/mL), and cells were incubated for 1 h. Thereafter, the cells were scraped and transferred into 5 mL tubes. The tubes were briefly vortexed, and 100 μL of DLD1 cell suspension was transferred into a microcentrifuge tube containing 500 μL of a 75:25 mixture of silicon oil (density = 1.05) and mineral oil (density = 0.872). The mixture was centrifuged at 14000 rpm for 5 min. After the tubes were frozen with liquid nitrogen, the bottom tips containing the cell pellet were cut off. The cell pellets and the supernatants were counted with a γ-counter. The protein content in 100 μL of cell suspension was quantified using the Bio-Rad protein assay kit according to the manufacturer's protocol. The radioactivity in the cell pellets and media were counted. Activity ratios of the cell pellet to medium ([cpm/μg protein in pellet]/[cpm/μg medium]) were calculated and plotted against TRAIL concentration. The experiments were performed five times.

Flow Cytometry with Apoptotic Cells. DLD1 cells at a concentration of 10^6 cell/mL were incubated with 150 ng/mL of TRAIL for 2 h at 37 °C to induce apoptosis. The percentage of apoptotic cells was estimated by staining with annexin V-FAM and propidium iodide and found to be greater than 50%. DLD1 cells without TRAIL treatment were used as a control. After removal of TRAIL, both TRAIL-treated and untreated cells were incubated with 20 μM FAM-labeled peptide for 15 min at room temperature. Thereafter, the medium was replaced with RPMI 1640 medium with no phenol red. For competition experiments,

the TRAIL-treated DLD1 cells were incubated with 20 μM FAM-labeled peptide for 15 min at room temperature. After they were washed once with PBS, the cells were incubated with 500 μL of 5 μM annexin V in binding buffer (10 mM HEPES, 140 mM NaCl, and 2.5 mM $CaCl_2$ at pH 7.4) for another 15 min at room temperature. The medium was then replaced with RPMI1640 free of phenol red. The cells were analyzed on a Becton-Dickinson FACS Calibur benchtop flow cytometer (BD Biosciences, San Jose, CA) equipped with an air-cooled 15 mW 488 nm argon ion laser. The FAM-peptide was detected through a 530/30 nm filter, and data were acquired with CellQuest acquisition software, version 3.3 (BD Biosciences). All fluorescence measurements were made on a four-decade log scale.

Fluorescence Microscopy. DLD1 cells were seeded (1×10^4/well) in a 96-well plate (Corning, Lowell, MA) supplemented with RPMI 1640 medium containing 10% fetal bovine serum. Apoptosis was induced by treating cells with TRAIL (150 ng/mL) for 2 h at 37 °C. The supernatant was collected in conical tubes, while the remaining treated cells were trypsinized, added to the floating cell population, and spun down. The untreated viable cells were trypsinized and collected, and the cells were centrifuged at 3000 rpm for 5 min. The pellets were washed with RPMI 1640 without phenol red. Both apoptotic and viable cells were incubated with either FAM-SAAC(Re)-PSBP-6 or FAM-scrambled PSBP-0 peptide (final concentration 10 μM) for 15 min at 4 °C, and then, each peptide was replaced with 200 μL of Hanks' balanced salt solution plus 2.5 mM $CaCl_2$ and 2.5 μL of Alexa Fluor 594-labeled annexin V (Invitrogen), and cells were incubated for 15 min at room temperature. After they were washed with RPMI 1640, the cells were transferred into Lab-Tek II chambered cover glass (Nalge Nunc International, Naperville, IL) and visualized using a Zeiss Axio Observer. Z1 fluorescence microscope equipped with a charge-coupled device camera (Carl Zeiss MicroImaging GmbH, Göttingen, Germany). The filters with Ex/Em 495/519 and 590/617 nm were used to visualize FAM-labeled peptide and Alexa Fluor 594-labeled annexin V, respectively. The cell morphology was visualized under bright field using differential interference contrast imaging.

Biodistribution, Autoradiography, and Immunohistochemistry. For biodistribution study, nude mice were inoculated subcutaneously with 5×10^5 B16/F10 murine melanoma cells (ATCC). When tumors had grown to ~10−12 mm in diameter, mice were randomly allocated into two groups. Mice in group 1 were treated intravenously with PG-TXL at a dose of 100 mg equivalent paclitaxel/kg ($n = 5$); mice in group 2 were left untreated ($n = 4$). Twenty-four hours later, all mice were injected intravenously with 15−20 μCi/mouse of SAAC(^{99m}Tc)-PSBP-6. After 4 h, mice were killed with CO_2 exposure. The organs of interest were excised and weighed, and radioactivity was counted in a γ-counter. The stomach and intestines were emptied of food contents prior to radioactivity measurements. The percentage of injected dose per gram (% ID/g) was calculated by dividing the % ID/organ by the weight of the tissue.

For autoradiographic studies, the tumors were cryosectioned (thickness, 5 μm), and the slices were dried at 40 °C in open air. The sections were then photographed and exposed on BAS-SR 2025 Fuji phosphorus film, and the film was scanned with FLA5100 Multifunctional Imaging System (Fujifilm Medical Systems USA, Stamford, CT). One slice from each tumor was stained with hematoxylin and eosin. An adjacent slice was stained with terminal deoxynucleotidyl transferase (TdT)-mediated dUTP nick end labeling (TUNEL) (TACS TdT in situ-fluorescein, R&D Systems, Minneapolis, MN) according to the manufacturer's protocol. The cell nuclei were counterstained with 4′,6-diamidino-2-phenylindole (DAPI, Sigma). TUNEL-stained slides were visualized under a fluorescence microscope (Zeiss Axio Observer.Z1).

AUTHOR INFORMATION

Corresponding Author

*Tel: 713-792-5182. Fax: 713-794-5456. E-mail: cli@mdanderson.org.

ACKNOWLEDGMENT

We thank Stephanie Deming for editing the article and Dr. John McMurray for helpful discussions. This work was supported in part by the John S. Dunn Foundation.

ABBREVIATIONS USED

DAPI, 4′,6-diamidino-2-phenylindole; FACS, fluorescence-activated cell sorting; FAM, 5-carboxyfluorescein; HOBt, 1-hydroxybenzotriazole; HPLC, high-performance liquid chromatography; HRMS-ESI, high-resolution electrospray ionization mass spectrometry; K_a, association constant; K_d, dissociation constant; PBS, phosphate-buffered saline; PC, phosphatidylcholine; PS, phosphatidylserine; PE, phosphatidylethanolamine; PG-TXL, poly(L-glutamic acid)-paclitaxel; PSBP-0, the first generation PS-binding peptide (FNFRLKAGQKIRFG); RUs, response units; Ala, alanine; SAAC, single amino acid chelator; SPR, surface plasmon resonance; ^{99m}Tc, technetium-99 m; Re, rhenium; TRAIL, tumor necrosis factor-related apoptosis-inducing ligand; TUNEL, terminal deoxynucleotidyl transferase-mediated dUTP nick end labeling

REFERENCES

(1) Riedl, S. J.; Shi, Y. Molecular mechanisms of caspase regulation during apoptosis. *Nat. Rev. Mol. Cell Biol.* **2004**, *5*, 897–907.

(2) Shi, Y. A structural view of mitochondria-mediated apoptosis. *Nat. Struct. Biol.* **2001**, *8*, 394–401.

(3) Kim, R.; Tanabe, K.; Uchida, Y.; Emi, M.; Inoue, H.; Toge, T. Current status of the molecular mechanisms of anticancer drug-induced apoptosis. The contribution of molecular-level analysis to cancer chemotherapy. *Cancer Chemother. Pharmacol.* **2002**, *50*, 343–352.

(4) Kang, M. H.; Reynolds, C. P. Bcl-2 Inhibitors: Targeting mitochondrial apoptotic pathways in cancer therapy. *Clin. Cancer Res.* **2009**, *15*, 1126–1132.

(5) Van Den Eijnde, S. M.; Boshart, L.; Baehrecke, E. H.; De Zeeuw, C. I.; Reutelingsperger, C. P. M.; Vermeij-Keers, C. Cell surface exposure of phosphatidylserine during apoptosis is phylogenetically conserved. *Apoptosis* **1998**, *3*, 9–16.

(6) Hanshaw, R. G.; Smith, B. D. New reagents for phosphatidylserine recognition and detection of apoptosis. *Bioorg. Med. Chem.* **2005**, *13*, 5035–5042.

(7) Kenis, H.; Hofstra, L.; Reutelingsperger, C. P. M. Annexin A5: Shifting from a diagnostic towards a therapeutic realm. *Cell. Mol. Life Sci.* **2007**, *64*, 2859–2862.

(8) Vanderheyden, J. L.; Liu, G.; He, J.; Patel, B.; Tait, J. F.; Hnatowich, D. J. Evaluation of ^{99m}Tc-MAG3-annexin V: Influence of the chelate on in vitro and in vivo properties in mice. *Nucl. Med. Biol.* **2006**, *33*, 135–144.

(9) Tait, J. F.; Smith, C.; Blankenberg, F. G. Structural requirements for In Vivo detection of cell death with ^{99m}Tc-annexin V. *J. Nucl. Med.* **2005**, *46*, 807–815.

(10) Prinzen, L.; Miserus, R.-J. J. H. M.; Dirksen, A.; Hackeng, T. M.; Deckers, N.; Bitsch, N. J.; Megens; Douma, K.; Heemskerk, J. W.; Kooi, M. E.; Frederik, P. M.; Slaaf, D. W.; van Zandvoort, M. A. M. J.; Reutelingsperger, C. P. M. Optical and magnetic resonance imaging of cell death and platelet activation using Annexin A5-functionalized quantum dots. *Nano Lett.* **2006**, *7*, 93–100.

(11) Schellenberger, E. A.; Weissleder, R.; Josephson, L. Optimal modification of annexin V with fluorescent dyes. *ChemBioChem* **2004**, *5*, 271–274.

(12) Blankenberg, F. G.; Tait, J.; Ohtsuki, K.; Strauss, H. W. Apoptosis: The importance of nuclear medicine. *Nucl. Med. Commun.* **2000**, *21*, 241–250.

(13) Ke, S.; Wen, X.; Wu, Q. P.; Wallace, S.; Charnsangavej, C.; Stachowiak, A. M.; Stephens, C. L.; Abbruzzese, J. L.; Podoloff, D. A.;

Li, C. Imaging taxane-induced tumor apoptosis using PEGylated, ^{111}In-labeled annexin V. *J. Nucl. Med.* **2004**, *45*, 108–115.

(14) Quinti, L.; Weissleder, R.; Tung, C.-H. A fluorescent nanosensor for apoptotic cells. *Nano Lett.* **2006**, *6*, 488–490.

(15) Thapa, N.; Kim, S.; So, I.-S.; Lee, B.-H.; Kwon, I.-C.; Choi, K.; Kim, I.-S. Discovery of a phosphatidylserine-recognizing peptide and its utility in molecular imaging of tumour apoptosis. *J. Cell Mol. Med.* **2008**, *12*, 1649–1660.

(16) Shao, R.-P.; Xiong, C.; Wen, X.-X.; Gelovani, J. G.; Li, C. Targeting phosphatidylserine on apoptotic cells with phages and peptides selected from a bacteriophage display library. *Mol. Imaging* **2007**, *6*, 417–426.

(17) Igarashi, K.; Kaneda, M.; Yamaji, A.; Saido, T. C.; Kikkawa, U.; Ono, Y.; Inoue, K.; Umeda, M. A novel phosphatidylserine-binding peptide motif defined by an anti-idiotypic monoclonal antibody. Localization of phosphatidylserine-specific binding sites on protein kinase C and phosphatidylserine decarboxylase. *J. Biol. Chem.* **1995**, *270*, 29075–29078.

(18) Cooper, M. A. Optical biosensors in drug discovery. *Nat. Rev. Drug Discovery* **2002**, *1*, 515–528.

(19) Homola, J. Surface plasmon resonance sensors for detection of chemical and biological species. *Chem. Rev.* **2008**, *108*, 462–493.

(20) Rich, R. L.; Myszka, D. G. Survey of the year 2006 commercial optical biosensor literature. *J. Mol. Recognit.* **2007**, *20*, 300–366.

(21) Erb, E.-M.; Chen, X.; Allen, S.; Roberts, C. J.; Tendler, S. J. B.; Davies, M. C.; Forsén, S. Characterization of the surfaces generated by liposome binding to the modified dextran matrix of a surface plasmon resonance sensor chip. *Anal. Biochem.* **2000**, *280*, 29–35.

(22) Rich, R. L.; Myszka, D. G. Survey of the year 2005 commercial optical biosensor literature. *J. Mol. Recognit.* **2006**, *19*, 478–534.

(23) Jiang, J.; Prasad, K.; Lafer, E. M.; Sousa, R. Structural basis of interdomain communication in the Hsc70 chaperone. *Mol. Cell* **2005**, *20*, 513–524.

(24) Geuijen, C. A. W.; Clijsters-van der Horst, M.; Cox, F.; Rood, P. M. L.; Throsby, M.; Jongeneelen, M. A. C.; Backus, H. H. J.; van Deventer, E.; Kruisbeek, A. M.; Goudsmit, J.; de Kruif, J. Affinity ranking of antibodies using flow cytometry: Application in antibody phage display-based target discovery. *J. Immunol. Methods* **2005**, *302*, 68–77.

(25) Biancone, L.; Schillaci, O.; Capoccetti, F.; Bozzi, R. M.; Fina, D.; Petruzziello, C.; Geremia, A.; Simonetti, G.; Pallone, F. Technetium-^{99m}-HMPAO labeled leukocyte single photon emission computerized tomography (SPECT) for assessing Crohn's disease extent and intestinal infiltration. *Am. J. Gastroenterol.* **2005**, *100*, 344–354.

(26) De Boer, J.; Slart, R. H. J. A.; Blanksma, P. K.; Willemsen, A. T. M.; Jager, P. L.; Paans, A. M. J.; Vaalburg, W.; Piers, D. A. Comparison of ^{99m}Tc-sestamibi-^{18}F-fluorodeoxyglucose dual isotope simultaneous acquisition and rest-stress ^{99m}Tc-sestamibi single photon emission computed tomography for the assessment of myocardial viability. *Nucl. Med. Commun.* **2003**, *24*, 251–257.

(27) Lavely, W. C.; Goetze, S.; Friedman, K. P.; Leal, J. P.; Zhang, Z.; Garret-Mayer, E.; Dackiw, A. P.; Tufano, R. P.; Zeiger, M. A.; Ziessman, H. A. Comparison of SPECT/CT, SPECT, and planar imaging with single- and dual-phase (99m)Tc-sestamibi parathyroid scintigraphy. *J. Nucl. Med.* **2007**, *48*, 1084–1089.

(28) Levadala, M. K.; Banerjee, S. R.; Maresca, K. P.; Babich, J. W.; Zubieta, J. Direct reductive alkylation of amino acids: Synthesis of bifunctional chelates for nuclear imaging. *Synthesis* **2004**, 1759–1766.

(29) Stephenson, K. A.; Banerjee, S. R.; Besanger, T.; Sogbein, O. O.; Levadala, M. K.; McFarlane, N.; Lemon, J. A.; Boreham, D. R.; Maresca, K. P.; Brennan, J. D.; Babich, J. W.; Zubieta, J.; Valliant, J. F. Bridging the gap between in vitro and In Vivo imaging: Isostructural Re and ^{99m}Tc complexes for correlating fluorescence and radioimaging studies. *J. Am. Chem. Soc.* **2004**, *126*, 8598–8599.

(30) Bayly, S. R.; Fisher, C. L.; Storr, T.; Adam, M. J.; Orvig, C. Carbohydrate conjugates for molecular imaging and radiotherapy: ^{99m}Tc(I) and ^{186}Re(I) tricarbonyl complexes of N-(2′-hydroxybenzyl)-2-amino-2-deoxy-D-glucose. *Bioconjugate Chem.* **2004**, *15*, 923–926.

(31) Gazitt, Y. TRAIL is a potent inducer of apoptosis in myeloma cells derived from multiple myeloma patients and is not cytotoxic to hematopoietic stem cells. *Leukemia* **1999**, *13*, 1817–1824.

(32) Corsten, M. F.; Hofstra, L.; Narula, J.; Reutelingsperger, C. P. M. Counting Heads in the War against Cancer: Defining the Role of Annexin A5 Imaging in Cancer Treatment and Surveillance. *Cancer Res.* **2006**, *66*, 1255–1260.

(33) Alberto, R.; Egli, A.; Abram, U.; Hegetschweiler, K.; Gramlich, V.; Schubiger, P. A. Synthesis and reactivity of $[NEt_4]_2[ReBr_3(CO)_3]$. Formation and structural characterization of the clusters $[NEt_4][Re_3(\mu_3\text{-}OH)(\mu\text{-}OH)_3(CO)_9]$ and $[NEt_4][Re_2(\mu\text{-}OH)_3(CO)_6]$ by alkaline treatment. *J. Chem. Soc., Dalton Trans.: Inorg. Chem.* **1994**, 2815–2820.